bond angles modify dramatically the ligand field around the cobalt ion. On the basis of the calculated values therefore we assign the experimental g values to the principal directions as shown in Table II.

In order to have the correct parameters for the $\hat{H}_{Co}$ Hamiltonian, we recalculated the g values also within this simplified model. The best fit values are $g_x = 6.1$, $g_y = 2.0$, and $g_z = 3.4$, with the paramters fixed at $\gamma = -1.5$, $\zeta = 533$ cm^{-1}, $D_{Co} = -877$ cm^{-1}, $E_{Co} = 246$ cm^{-1}, and $k = 1$.

The third step was that of calculating, with the parameters for $\hat{H}_{Co}$ and $\hat{H}_{Ni}$ fixed as shown above, the g values of the Ni–Co pair. A 36 × 36 matrix for the $^4T_{1g} \times {}^3A_{2g}$ manifold was calculated, which by diagonalization gave a spectrum of eigenvalues and eigenvectors. The g values within the lowest Kramers doublet were calculated with the Zeeman Hamiltonian:

$$\hat{H}_Z = \mu_B B(k\hat{L}_{Co} + g_e\hat{S}_{Co}) + \mu_B B g_{Ni}\cdot\hat{S}_{Ni} \qquad (6)$$

The calculated g values for several sets of values of the J_{A_1} J_{A_2}, and J_{B_2} parameters are shown in Figure 7. It is apparent that the parameter that determines the largest variation of the g values is J_{B_2}. The calculations were performed also with different zero-field splitting parameters of the nickel(II) ion, since in the procedure outlined above they were found to depend to some extent on the angular overlap parameters. The calculated g values of the Ni–Co pair, however, were found to be relatively insensitive to the actual values of D_{Ni} and E_{Ni} used.

The best fit parameters are $J_{A_1} = 30 \pm 10$ cm^{-1}, $J_{A_2} = 30 \pm 10$ cm^{-1}, and $J_{B_2} = 30 \pm 10$ cm^{-1}. The g values computed with these parameters fixed at 30 cm^{-1} are $g_x = 1.0$, $g_y = 2.1$, and $g_z = 0.6$. Comparing them to the values for the trik complexes shows that the J_{A_2} and J_{B_2} parameters are only slightly smaller in the present case, while J_{A_1} is definitely larger. It is worth mentioning that in the nickel dhph complex J was estimated to be 92 cm^{-1}, while it was 30 cm^{-1} in the nickel trik complex.

The A_1, A_2, and B_2 pathways are, to a good approximation, determined according to the relations[34,35]

$$J_{A_1} = \tfrac{1}{6}(J_{xy,xy} + J_{xy,z^2} + J_{xy,x^2-y^2} + J_{z^2,z^2} + J_{z^2,xy} + J_{z^2,x^2-y^2})$$

$$J_{A_2} = \tfrac{1}{6}(J_{xy,xy} + J_{xy,z^2} + J_{xy,yz} + J_{z^2,z^2} + J_{z^2,xy} + J_{z^2,yz}) \qquad (7)$$

$$J_{B_2} = \tfrac{1}{6}(J_{xy,xy} + J_{xy,z^2} + J_{xy,xz} + J_{z^2,z^2} + J_{z^2,xy} + J_{z^2,xz})$$

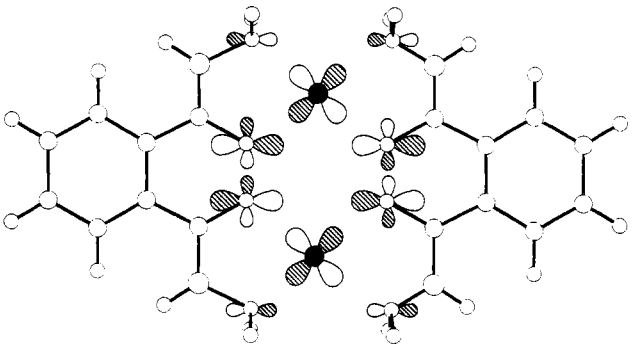

Figure 8. Symmetry of the highest occupied ligand and metal orbitals.

In (7) the first orbital is a nickel orbital, while the second one is a cobalt(II) orbital. Antiferromagnetic contributions are expected only for the couples of orbitals that span the same irreducible representation of C_{2v} symmetry. Therefore only $J_{xy,xy}$, J_{z^2,z^2}, J_{z^2,x^2-y^2} can be effective in determining antiferromagnetic coupling. Extended Hückel calculations on the ligand, for which an idealized C_s symmetry was assumed, show that the highest occupied ligand orbitals have the correct symmetry for determining an antiferromagnetic pathway, as shown in Figure 8. Overlap considerations suggest that the order of the coupling constants is $J_{xy,xy} > J_{z^2,z^2} > J_{z^2,x^2-y^2}$. Of the other exchange interactions J_{ij} the one that may bring some substantial ferromagnetic contribution is J_{xy,x^2-y^2}. As compared to the case of the Ni–Co trik pairs[14] this mechanism, however, should be less effective, because the two orbitals xy and $x^2 - y_2$ are further removed from each other since two metal ions are bridged by two atoms in the dhph ligand, while a monoatomic bridge was present in the trik complex. This might be the reason why in this case the three J values are essentially similar to each other, while in the case of the trik complex the J_{A_1} value, which included the ferromagnetic J_{xy,x^2-y^2} pathway, was substantially smaller than the others.

Acknowledgment. CNR Grant No 81.01630.03 is gratefully acknowledged. Thanks are expressed to Professor M. Di Vaira for helpful discussion on the extended Hückel calculations.

Registry No. $Ni_2(dhph)_2(H_2O)_4Cl_4$, 24686-50-8; Cu, 7440-50-8; Co, 7440-48-4.

(34) Anderson, P. W. *Solid State Phys.* **1963**, *14*, 99.
(35) Eremin, M. V.; Rakitin, Y. V. *Phys. Status Solidi B* **1977**, *80*, 579.

Contribution from the Laboratoire de Physicochimie Structurale, Université de Paris-Val de Marne, 94000 Creteil, France, and LURE,[1a] the Laboratoire de Physicochimie Minérale, and ERA 672, Université de Paris-Sud, 91405 Orsay Cedex, France

EXAFS Study of the Structural Modifications Induced into $MnPS_3$ upon Intercalation

A. MICHALOWICZ*[1b] and R. CLEMENT[1c]

Received February 4, 1982

EXAFS spectra have been recorded at the manganese K edge in the layered compound $MnPS_3$ and in two intercalation compounds containing cobaltocenium cations, at 15 and 300 K. The intercalation process is shown to induce local disorder or distortion in the structural environment of manganese, although the intercalates still have X-ray powder diffraction patterns typical of crystalline materials. These structural effects are discussed in relation to the magnetic properties of the intercalates.

Introduction

Transition-metal hexathiohypodiphosphates MPS_3, where M is a metal in the +2 oxidation state, form a class of lamellar,[2a] broad-band semiconductors[3] with an energy gap lying in the range 1.6–3.5 eV. Their structure[2] is related to that of $CdCl_2$, with metal ions and phosphorus–phosphorus pairs

(1) (a) LURE: CNRS laboratory associated with the Université de Paris-Sud. (b) Laboratoire de Physicochimie Structurale and LURE. (c) Laboratoire de Physicochimie Minérale and ERA 672.

(2) (a) Klingen, W.; Ott, R.; Hahn, H. *Z. Anorg. Allg. Chem.* **1973**, *396*, 271. (b) Klingen, W.; Eulenberger, G.; Hahn, H. *Ibid.* **1973**, *401* 97.
(3) Brec, R.; Schleich, D. M.; Ouvrard, G.; Louisy, A.; Rouxel, J. *Inorg. Chem.* **1979**, *18*, 1814.

0020-1669/82/1321-3872$01.25/0

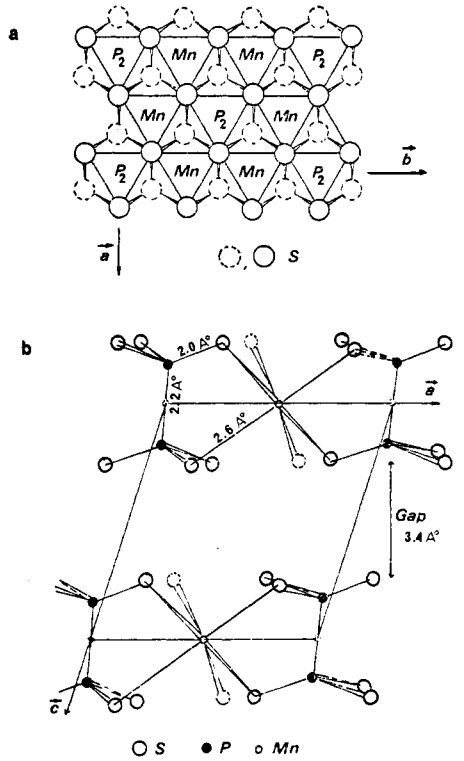

Figure 1. (a) Structural model of an $MnPS_3$ layer, showing the $\vec{a}$ and $\vec{b}$ axes of the monoclinic unit cell. (b) Perspective view of the monoclinic unit cell of $MnPS_3$. The $\vec{b}$ axis is perpendicular to the plane of the figure.

occupying the cadmium positions and sulfur atoms occupying the chloride positions (Figure 1). Interest in these materials has been initially centered around their use as solid-state cathodes,[4] but it has been recently realized that the MPS_3 compounds have an original intercalation chemistry which yields intercalates of potential interest.[5-7] Two classes of MPS_3 intercalates have been described: (i) those obtained upon reaction with reducing, electron donor species, with several MPS_3 intercalating lithium,[3,4] either chemically or electrochemically, as well as electropositive metallocenes[8] such as cobaltocene; (ii) those obtained through an unusual cation-transfer process,[9] with $MnPS_3$ being capable of taking up certain cationic species from an aqueous solution and incorporating them into the interlayer space, while a corresponding amount of intralayer manganese cations are expelled into the solution, thus balancing electric charges.

In a previous article,[6] we have shown that intercalating $MnPS_3$ with metallocenes resulted in a dramatic modification of the magnetic properties of the material: the intraplanar antiferromagnetic coupling between Mn^{2+} ions was reduced, and a spontaneous magnetization occurred below ~40 K in the intercalates. It is remarkable that the same modifications were observed, no matter which route—reduction or cation transfer—was used to prepare the intercalation compounds. Unfortunately, little is known about the structural modifications caused by intercalation. Although such data would be highly desirable for an understanding of the magnetic properties (which may be very sensitive to minor structural changes), the quasi-impossibility of getting suitable crystals of the intercalated materials makes it very difficult to obtain detailed structural information by X-ray crystallography. As shown below, the X-ray powder patterns show that the periods within the layers are almost unaffected by intercalation; yet this only reflects the fact that the stacking of the sulfur atoms is not upset and it does not bring any information about possible changes of the local environment of the manganese and phosphorus atoms. Therefore, the study of the extended X-ray absorption fine structure (EXAFS) of manganese in these materials seemed to us an appropriate means to increase our understanding of the short-range order around the manganese ions. Thus, we undertook a comparative EXAFS study of $MnPS_3$ and two derived intercalation compounds, one synthesized by reaction with neutral cobaltocene, $MnPS_3[Co(C_5H_5)_2]_{0.34}$, (electron-transfer route), the other one obtained by reaction with an aqueous solution of cobaltocenium iodide, $Mn_{0.83}PS_3[Co(C_5H_5)_2]_{0.34}$ (cation-transfer route). Previous spectroscopic work[10] has clearly shown that in both cases the guest species are cationic. The negative charge on the layers arises from localized electrons in the former case and from manganese cation deficiency in the latter case. Both intercalates exhibit almost identical data (UV–visible and IR spectra, X-ray powder patterns, magnetic properties), so that their comparative EXAFS study seemed particularly attractive. We note here that the only EXAFS study of lamellar intercalation compounds containing transition metals reported so far concerned Rb_xNbSe_2 intercalates and that it merely concluded to slight modifications of the Nb–Nb distances upon intercalation.[11]

Table I. Indexation of $Mn_{0.84}PS_3[Co(C_5H_5)_2]_{0.34}$[a]

I	d_{exptl}, Å	d_{calcd}, Å	hkl
M	11.85	11.85	001
M	5.926	5.925	002
S	5.293	5.295	020
W	3.952	3.950	003
S	3.014	3.015	130 (20$\bar{2}$)
W	2.964	2.962	004
M	2.892	2.892	200 (13$\bar{2}$)
S	2.809	2.809	131
S	2.519	2.519	132
M	2.317	2.318	202
M	2.221	2.221	133
M	2.103	2.104	23$\bar{1}$
M	2.036	2.039	30$\bar{2}$
F	1.765	1.766	06$\bar{0}$ (33$\bar{2}$)
F	1.745	1.746	33$\bar{1}$ (061)
M	1.692	1.692	330 (062)
W	1.612	1.612	33$\bar{1}$
W	1.525	1.527	26$\bar{2}$
M	1.494	1.495	40$\bar{1}$
M	1.445	1.446	400

[a] d_{exptl} = spacings experimentally found; d_{calcd} = spacings calculated on the basis of the monoclinic unit cell described in the text. The relative intensities (I) are described as W (weak), M (medium), and S (strong).

Experimental Section and Results

Synthesis. The synthesis of pure $MnPS_3$ has already been described, as well as the synthesis and characterization of the intercalation compounds $MnPS_3[Co(C_5H_5)_2]_{0.34}$ (I) and $Mn_{0.83}PS_3[Co(C_5H_5)_2]_{0.34}$ (II).[6]

X-ray Powder Diffraction. The crystallographic characterization reported so far for intercalates I and II only deals with the increase of the interlamellar spacing upon interca-

(4) Le Mehaute, A.; Ouvrard, G.; Brec, R.; Rouxel, J. *Mater. Res. Bull.* **1977**, *12*, 1191.
(5) Clement, R. *J. Am. Chem. Soc.* **1981**, *103*, 6998.
(6) Clement, R.; Girerd, J. J.; Morgenstern-Badarau, I. *Inorg. Chem.* **1980**, *19*, 2852.
(7) Clement, R.; Garnier, O.; Mathey, Y. *Nouv. J. Chim.* **1982**, *6*, 13.
(8) Clement, R.; Green, M. L. H. *J. Chem. Soc., Dalton Trans.* **1979**, *10*, 1566.
(9) Clement, R. *J. Chem. Soc., Chem. Commun.* **1980**, 647.
(10) Mathey, Y.; Clement, R.; Sourisseau, C.; Lucazeau, G. *Inorg. Chem.* **1980**, *19*, 2773.
(11) Bourdillon, A. J.; Pettifer, R. F.; Marseglia, E. A. *Physica B+C (Amsterdam)* **1980**, *99B+C*, 64.

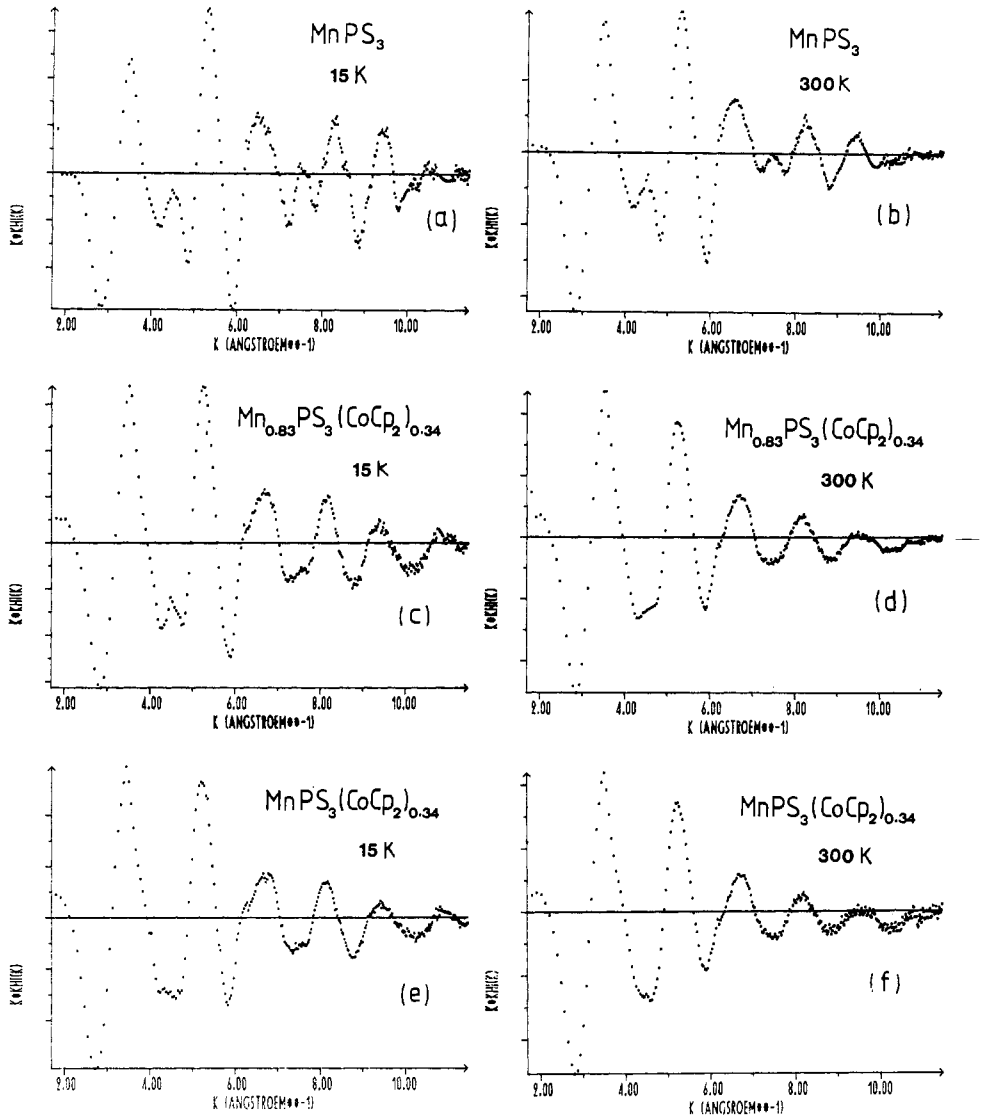

Figure 2. $k[\chi(k)]$ EXAFS oscillations for $MnPS_3$ at 15 (a) and 300 K (b), $M_{0.83}PS_3[Co(C_5H_5)_2]_{0.34}$ at 15 (c) and 300 K (d), and $MnPS_3$-$[Co(C_5H_5)_2]_{0.34}$ at 15 (e) and 300 K (f)

lation, and no unit cell has been published yet. X-ray powder diffraction photographs of $MnPS_3$ and of the intercalates I and II were taken with use of an asymmetric Seeman-Bohlin camera and Cu $K\alpha_1$ radiation.

Pure $MnPS_3$ exhibits very sharp reflections, which can be indexed in the monoclinic unit cell (see Figure 1) previously described,[2] with the following parameters: $a = 6.087$ Å, $b = 10.53$ Å, $c = 6.80$ Å, $\beta = 107.1°$.

The pattern of intercalate I is essentially identical with the pattern of II; both of them exhibit sharp reflections, which are collected in Table I. All reflections can be indexed (within ±0.001 Å) on the basis of a monoclinic unit cell closely related to the unit cell of $MnPS_3$, with nearly the same a and b parameters within the layers while the c parameters strongly increases as a consequence of intercalation. The following set has been obtained: $a = 6.117$ Å, $b = 10.59$ Å, $c = 12.53$ Å, $\beta = 109.0°$. Thus although no information concerning possible local disorder can be drawn from this study, it is obvious that the intercalates are still crystalline, three-dimensionally ordered materials and that the sulfur atom stacking, which constitutes the skeleton of the layers, is conserved upon intercalation.

EXAFS Study. EXAFS spectra of $MnPS_3$ and of intercalates I and II at the manganese K edge have been recorded at LURE, the French synchrotron radiation laboratory, with use of the X-ray absorption spectrometer of the DCI storage ring described by Raoux et al.[12] The samples consist of thin sheets (20 × 5 mm², 8 mg) of powder fixed on Celotape. Each spectrum is the sum of three independent recordings added after individual inspection. Spectra have been recorded both at room temperature and at 15 K. The different steps of our EXAFS analysis have used well-known techniques already described.[13]

The $k[\chi(k)]$ EXAFS oscillations are presented in Figure 2. Such curves are obtained after removal of the pre- and postedge background from the experimental absorption curves ($\ln (I_0/I)$ vs. the photon energy $h\nu$), followed by a transformation from $h\nu$ to

$$k = \left[\frac{2me}{\hbar^2}(h\nu - E_0)\right]^{1/2}$$

$E_0 = 6595$ eV for manganese

The radial distribution functions $\tilde{F}(R)$, obtained by Fourier transform of $k^3[\chi(k)]$ from k space to R space, are given in

(12) Raoux, D.; Petiau, J.; Bondot, P.; Calas, G.; Fontaine, A.; Lagarde, P.; Levitz, P.; Loupias, G.; Sadoc, A. *Rev. Phys. Appl.* **1980**, *15*, 1079.
(13) (a) Lytle, F. W.; Sayers, D. E.; Stern, E. A. *Phys. Rev. B: Solid State* **1975**, *11*, 4825. (b) Stern, E. A.; Sayers, D. E.; Lytle, F. W. *Solid State Ibid.* **1975**, *11*, 4836. (c) Brown, G. S.; Doniach, S. In "Synchrotron Radiation Research"; Winick, J. Doniach, S., Eds.; Plenum Press: New York, **1981**; p 353–383. (d) Teo, B. K. In "Exafs Spectroscopy"; Teo, B. K., Joy, D. C., Eds.; Plenum Press New York, 1981; p 13–58.

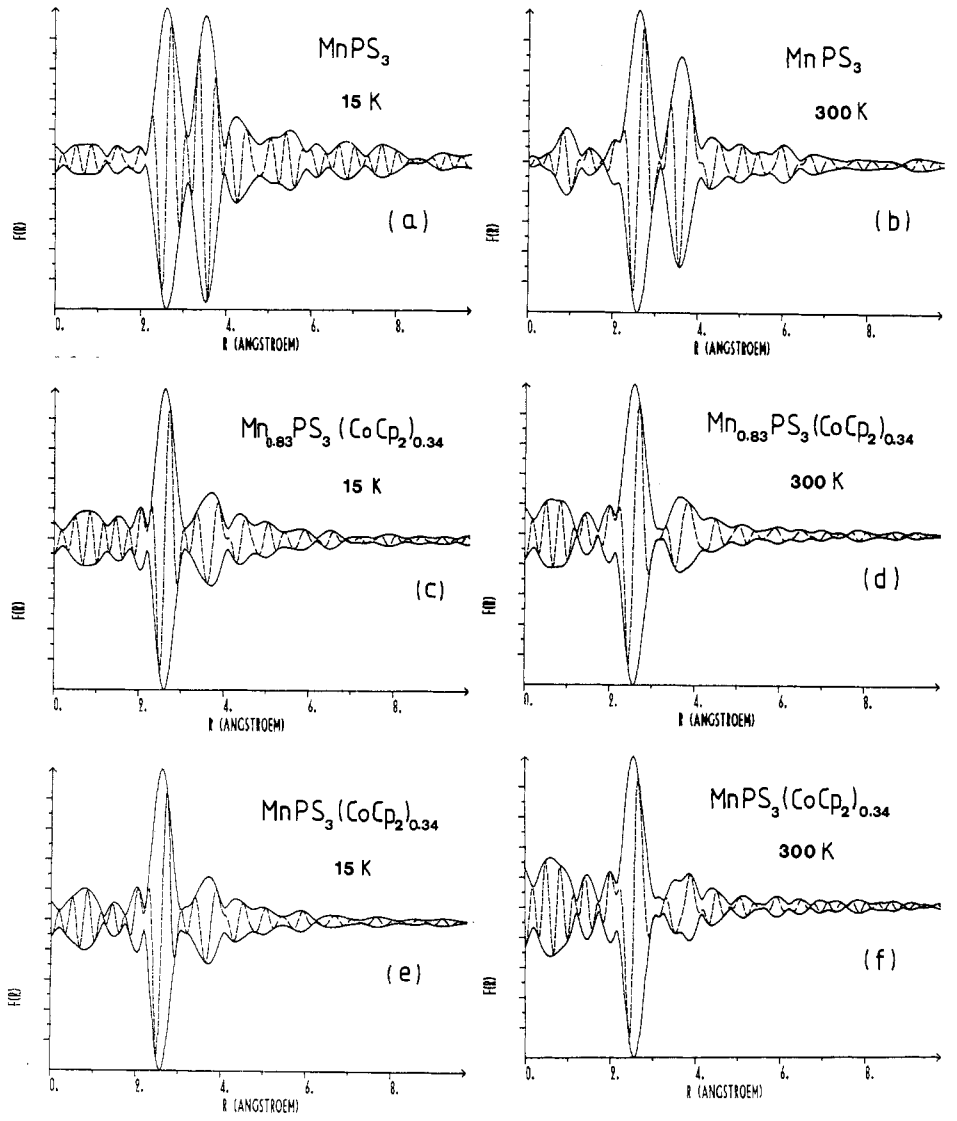

Figure 3. Real part (broken line) and modulus (full line) of the Fourier transform FT ($k^3[\chi(k)]e^{-i[\varphi(k)]}$), where $\varphi(k)$ is the manganese–sulfur phase shift and where the E_0 threshold is varied until the maximum of the imaginary part $I_m[F(R)]$ and the maximum of the modulus $F(R)$ are in coincidence (Lee and Beni criterion[19] for the determination of single-shell distance): $MnPS_3$ at 15 (a) and 300 K (b), $Mn_{0.83}PS_3[Co(C_5H_5)_2]_{0.34}$ at 15 (c) and 300 K (d), and $MnPS_3[Co(C_5H_5)_2]^{0.34}$ at 15 (e) and 300 K (f).

Figure 3. On these curves, each atomic shell surrounding the manganese atoms is represented by a peak. With the assumption that the crystal structure of $MnPS_3$ is isomorphous to that of $FePS_3$, the theoretical radial distribution for $MnPS_3$ may be easily calculated. Each manganese is surrounded by six sulfur atoms at 2.60 Å, three manganese atoms at 3.51 Å, and six phosphorus atoms at 3.68 Å. Thus, the first peak of the $\tilde{F}(R)$ curves for pure $MnPS_3$ (Figure 3a,b) is obviously related to the Mn–S distances, whereas the second one arises from the unresolved Mn–Mn and Mn–P distances.

Inspection of Figure 3 immediately reveals that the peak arising from Mn–Mn and Mn–P distances is drastically reduced when $MnPS_3$ is intercalated. Although less spectacular, we note that increasing the temperature of pure $MnPS_3$ from 15 to 300 K also results in a decrease of the EXAFS peaks, particularly of the second one, compared to the first one. The reason for such effects is clear: when the mean square fluctuation of an interatomic distance σ_i^2 increases, the corresponding EXAFS contribution decreases. Thus, intercalation induces some local disorder in the second shell (Mn–Mn, Mn–P) surrounding the manganese ions: we note that both intercalates exhibit similar disorder effects, which therefore cannot only be explained by the creation of manganese vacancies, as there is no manganese loss in I.

In order to quantify the increase of σ^2, we attempted a fitting of the k-space spectra to the classical formula (1). In this

$$k[\chi(k)] = \sum_i \frac{[f_i(k)]N_i}{R_i^2} \sin [2kR_i + \alpha_i(k)]e^{-2\sigma_i^2k^2}e^{-2R_i/\lambda} \quad (1)$$

formula, $\chi(k) = (\mu - \mu_0)/\mu_0$ is the normalized oscillatory component of the absorption coefficient, N_i is the number of neighbors at a distance R_i (6, 6, and 3 for the S, P, and Mn shells, respectively), λ is the mean free path of the photoelectron, $f_i(k)$ and $\alpha_i(k)$ are the amplitude and phase shift functions characteristic of the ejection of an electron from the central atom and its back-scattering by the neighbors (we used the tabulated values of Teo et al.[14]), and σ_i is a damping coefficient due to thermal vibration and distance distortions of the shell. Three parameters, σ_i, R_i, and E_0, are fitted per shell. The problem of correlations between fitted parameters occurring frequently in multishell analysis[15] was reduced by using the following procedure: (a) Fourier filtering of the first

(14) (a) Teo, B. K.; Lee, P. A.; Simons, A. L.; Eisenberger, P.; Kincaid, B. M. *J. Am. Chem. Soc.* **1977**, *99*, 3854. (b) Teo, B. K.; Lee, P. A.; Simons, A. L. *Ibid.* **1977**, *99*, 3856.

(15) Teo, B. K.; Eisenberger, P.; Kincaid, B. M. *J. Am. Chem. Soc.*, **1978**, *100*, 1735.

Table II. Fitting Results[a]

compd	temp, K	Mn-S σ, Å	Mn-S R, Å	Mn-P σ, Å	Mn-P R, Å	Mn-Mn σ, Å	Mn-Mn R, Å	% ρ
$MnPS_3$	15	0.03	2.60	0.03	3.69	0.02	3.48	0.3
	300	0.08	2.58	0.09	3.70	0.09	3.47	0.4
$Mn_{0.83}PS_3[Co(C_5H_5)_2]_{0.34}$	15	0.05	2.59	0.10	3.71	0.10	3.52	1.5
	300	0.10	2.57	0.16	3.72	0.16	3.51	0.9
$MnPS_3[Co(C_5H_5)_2]_{0.34}$	15	0.04	2.59	0.11	3.71	0.10	3.52	1.6
	300	0.11	2.56	0.17	3.71	0.17	3.53	1.8

[a] $\rho = \Sigma_k(\chi_{exptl} - \chi_{theor})^2/\Sigma_k(\chi_{exptl})^2$ is the three-shell-fit residual factor.

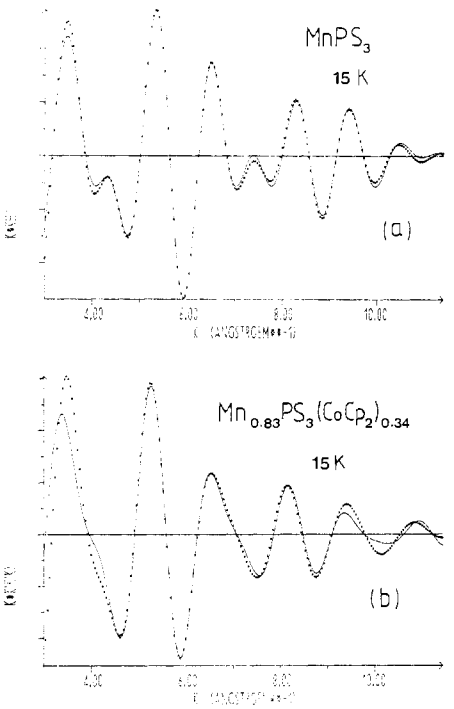

Figure 4. Least-squares fits (full lines) of back-transformed data (dotted line): (a) $MnPS_3$ at 15 K; (b) $Mn_{0.83}PS_3[Co(C_5H_5)_2]^{0.34}$ at 15 K. The figure shows two examples of fits to a two-peak (three shells) k-space spectrum.

shell and single-shell fit of the Mn–S contribution and (b) injection of the first shell results in the three-shell filtered spectrum and fit of the Mn–P and Mn–Mn parameters. The results of this two-step fitting procedure are given in Table II, and the fits of pure $MnPS_3$ and of intercalate II at 15 K are shown in Figure 4. It must be emphasized that the σ values presented here do not represent a unique mathematical solution; we have restained the σ_i on Mn–P and Mn–Mn to be approximately identical. Other choices were possible, for instance, $\sigma_{Mn} >> \sigma_P$, which gave good fits; our choice cannot be justified on the basis of the EXAFS data only and was guided by the X-ray diffraction results, which indicate that the periodicity of the layers is not much affected by intercalation (assuming a rigid sulfur matrix and a random Mn–S distance dispersion, one expects $\sigma_{Mn-P}^2 \simeq \sigma_{Mn-Mn}^2 \simeq 2\sigma_{Mn-S}^2$). Moreover, the use of eq 1 to extract distance dispersion data assumes the distance distribution to be Gaussian; the fact that R_{Mn-S} apparently decreases as σ_{Mn-S} increases is a classical symptom of a nonsymmetric distribution.[16] Therefore, although the results obtained should be considered as a semiquantitative approach only, the following points are nevertheless fairly well established: (i) intercalation of cobaltocenium cations into $MnPS_3$ induces some disorder in the local environment of manganese; (ii) this disorder is observable on the Mn–P, Mn–Mn, and even Mn–S distances, at 15 and 300 K; (iii) the Mn–S distance distribution is nonsymmetric, in both the pure and intercalated phases. The root mean square deviations induced by intercalation may be estimated by the quantity $(\sigma_{MnPS_3}^2 - \sigma_{intercalate}^2)^{1/2}$ for each shell and at each temperature (Table III). The values lie in the range 0.05–0.07 Å for Mn–S and 0.1–0.15 Å for the second and third shells. Again these numbers may be quantitatively crude but give a good qualitative picture of the structural change induced by intercalation.

(16) Eisenberger, P.; Brown, G. S. *Solid State Commun.* **1979**, *29*, 481.

Table III. Disorder Induced upon Intercalation of $MnPS_3$[a]

compd	temp, K	Δσ- (Mn-S)	Δσ- (Mn-P)	Δσ- (Mn-Mn)
$Mn_{0.83}PS_3[Co(C_5H_5)_2]_{0.34}$	15	0.04	0.10	0.10
	300	0.06	0.13	0.13
$MnPS_3[Co(C_5H_5)_2]_{0.34}$	15	0.03	0.10	0.10
	300	0.07	0.14	0.15

[a] For a particular distance, Δσ is defined as $(\sigma_{intercalate}^2 - \sigma_{MnPS_3}^2)^{1/2}$ and expressed in Å.

Discussion

The appearance of local disorder around the metallic cations in the layers underlines the originality of the MPS_3 materials with respect to the structurally analogous dichalcogenides $M'X_2$: indeed, our results contrast with those obtained for $NbSe_2$, where the intercalation of rubidium merely results in a slight Nb–Nb distance increase and does not induce any disorder in the niobium environment.[11]

The temperature dependence of the EXAFS spectra of $MnPS_3$ clearly reveals a nonsymmetric Mn–S distance distribution, which is indicative of loose bonding of the manganese ions. This is an important result, which corroborates previous conclusions drawn from infrared and Raman spectroscopy.[10] According to these techniques, $MnPS_3$ is best described as consisting of pyramidal PS_3 units with strong P–S bonds and of manganese ions loosely bound in the octahedral S_6 sites; in particular, no Mn–S vibrational mode could be seen, whereas translational modes of the manganese ions were identified at low frequency. The weak Mn–S bonding might be also a key factor governing the chemical reactivity of $MnPS_3$, allowing in particular intercalation through the departure of manganese ions from inside the layers.

If we turn now to the intercalates I and II, Table II shows that the mean square deviations of all distances have been significantly increased upon intercalation. This effect cannot be totally due to vibrations, as its importance is large even at 15 K. This means that the local geometry around the manganese atoms is slightly affected by intercalation. Unfortunately, it is not possible from the EXAFS results to establish whether (i) the manganese atoms are located in distorted sites in a regularly "puckered" layer or (ii) whether there exists a random distribution of differently distorted sites. It is worth pointing out here that the existence of distortions in the layer might be related to the splitting of the $\nu(PS_3)$ stretching mode observed in the IR spectra of the intercalates,[10] although this splitting may have another origin.

Finally, the EXAFS results give us a clue for understanding the magnetic properties of the intercalates, particularly the occurrence of spontaneous magnetization at low temperature; this magnetization has been ascribed to weak ferromagnetism,[6,17] a phenomenon that takes place when antiferromagnetically coupled spins do not align themselves exactly antiparallel, the canting resulting in an uncompensated macroscopic moment. The results described in the present study strongly suggest either that neighbor manganese ions see different environments or that the environments do not have the same orientation: as a consequence, the preferred directions of neighbor spins will not be parallel. Basically, the reason is that the "single-ion-anisotropy energy" is different for the same orientation of a spin at the two sites and that the total energy is minimized by a nonparallel arrangement.[18] This explanation seems more realistic than an invocation of antisymmetric exchange between the spins, which may be another source of canting. Although it is always very difficult to sort out the relative contributions of the two possible mechanisms, antisymmetric exchange is known to be small for Mn^{2+} ions, which have no first-order orbital magnetic contribution.

In conclusion, it turns out that EXAFS is a valuable technique to characterize local disorder in intercalated layers. Further EXAFS experiments on similar systems are in course, which should indicate whether the observed effects constitute a particular case or express some general feature of intercalation.

Acknowledgment. We thank the staff of the linear accelerator laboratory of Orsay, who operated the storage ring DCI for the synchrotron radiation dedicated shift used in this work. We also thank the staff of LURE, particularly those involved in the EXAFS spectrometer design. We are grateful to Dr. J. Goulon for his help in writing the EXAFS analysis programs and to Dr. R. Fourme for helpful discussions.

Registry No. I, 74346-92-2; II, 74346-93-3; $MnPS_3$, 20642-09-5.

(17) Clement, R.; Renard, J. P., to be submitted for publication.
(18) Carlin, R. L.; Van Duyneveldt, A. J. "Magnetic Properties of Transition Metal Compounds"; Springer-Verlag: New York, 1977.
(19) Lee, P.; Beni, G. *Phys. Rev. B: Solid State* **1977**, *15*, 2862.

Contribution from the Department of Chemistry, McMaster University, Hamilton, Ontario, Canada L8S 4M1

Vibrational Spectra and Analyses of the S_4^{2+}, Se_4^{2+}, Te_4^{2+}, and *trans*-$Te_2Se_2^{2+}$ Polyatomic Cations

ROBERT C. BURNS and RONALD J. GILLESPIE*

Received February 2, 1982

Raman and infrared spectra have been recorded on a number of compounds that contain the S_4^{2+}, Se_4^{2+}, Te_4^{2+}, and *trans*-$Te_2Se_2^{2+}$ polyatomic cations. In the case of S_4^{2+} isotopic enrichment of sulfur to 16.1% in ^{34}S has been used to help assign the fundamental vibrations of this cation on the basis of a square-planar structure with D_{4h} symmetry. Assignments have also been extended to the Se_4^{2+} and Te_4^{2+} cations. Differences with previous assignments are discussed. In the case of *trans*-$Te_2Se_2^{2+}$, assignments were made on the basis of a square-planar structure with D_{2h} symmetry. Extensive vibrational analyses, using a modified valence force field, have been carried out on all of these species, giving chalcogen–chalcogen stretching force constants (average values) of 2.69, 2.09, 1.41, and 1.78 mdyn/Å for S_4^{2+}, Se_4^{2+}, Te_4^{2+}, and *trans*-$Te_2Se_2^{2+}$, respectively. These values have been compared to values for chalcogen–chalcogen single bonds and are consistent with an expected formal bond order of 1.25 for these species. A brief treatment of the data for D_{4h} systems using central rather than valence force coordinates is also given.

Introduction

The polyatomic cations S_4^{2+}, Se_4^{2+}, and Te_4^{2+} and the polyatomic anion Bi_4^{2-}, each with 22 valence electrons, represent the only known examples of isolated homoatomic four-atom square-planar species that have D_{4h} symmetry.[1,2] This type of structure is important from the standpoint of vibrational analysis because of its inherent simplicity and has been treated on a theoretical basis by a number of researchers.[3,4] However, the only extensive treatments using normal-coordinate methods based on experimental work have been those by Gillespie and Pez,[5] and by Steudel[6] (who used the former's results) on the Se_4^{2+} cation. The rather limited extent to which the vibrational spectra of these species have been studied may, in part at least, be attributed to the difficulty in preparing compounds containing these species, which have been synthesized only in recent years. On the basis of the vibrational spectra obtained by Gillespie and co-workers, assignments have also been given for S_4^{2+} and Te_4^{2+}, but no normal-coordinate analyses have been made for these species.[1,7]

In both of the previous studies of Se_4^{2+} the vibrational data were interpreted in terms of the Urey–Bradley potential field and conflicting assignments were made for one of the fundamental modes of vibration. Furthermore, as part of a recent MO study of Te_4^{2+} using an ab initio pseudopotential approach, theoretically derived (symmetrized) force constants and vibrational frequencies were obtained that suggested an alternative assignment of the observed frequencies for this cation.[8] The purpose of the present work was to reinvestigate the vibrational spectra of the S_4^{2+}, Se_4^{2+}, and Te_4^{2+} cations and to carry out extensive vibrational analyses on each of these species. As an assist in the assignments isotopic substitution

(1) Gillespie, R. J.; Passmore, J. *Adv. Inorg. Chem. Radiochem.* **1975**, *17*, 49.
(2) Cisar, A.; Corbett, J. D. *Inorg. Chem.* **1977**, *16*, 2482.
(3) Pistorius, C. W. F. T. *Z. Phys. Chem. (Wiesbaden)* **1958**, *16*, 126.
(4) Cyvin, S. J. "Molecular Vibrations and Mean Square Amplitudes"; Elsevier: Amsterdam, 1968.
(5) Gillespie, R. J.; Pez, G. P. *Inorg. Chem.* **1969**, *8*, 1229.
(6) Steudel, R. *Z. Naturforsch., A* **1975**, *30A*, 1481.
(7) Gillespie, R. J.; Passmore, J.; Ummat, P. K.; Vaidya, O. C. *Inorg. Chem.* **1971**, *10*, 1327.
(8) Rothman, M. J.; Bartell, L. S.; Ewig, C. S.; Van Wazer, J. R. *J. Comput. Chem.* **1980**, *1*, 64.

0020-1669/82/1321-3877$01.25/0